Raman scattering study of H_2 trapped within {111}-oriented platelets in Si

M. Hiller, E. V. Lavrov,* and J. Weber
Technische Universität Dresden, 01062 Dresden, Germany

(Received 3 June 2009; revised manuscript received 16 June 2009; published 7 July 2009)

A Raman-scattering study of molecular hydrogen trapped within {111}-oriented platelets in Si is presented. The Raman lines originating from the rotational transitions $S_0(J)$ with $J=0$, 1, 2, and 3 are identified at 353(1), 587(1), 815(1), and 1034(2) cm^{-1}, respectively. At low temperatures, ortho-to-para conversion of H_2 trapped within platelets is observed and suggested to be caused by the interaction of H_2 molecules. The Raman band at 4150 cm^{-1} originates from vibrational transitions of H_2 within platelets. The shape of the band is composed of ortho- and para-H_2 species of two different platelet structures.

DOI: 10.1103/PhysRevB.80.045306 PACS number(s): 78.30.Am, 61.72.Nn, 61.72.uf, 63.20.Pw

I. INTRODUCTION

Hydrogen is a common and important impurity in semiconductors, which can be trapped at various sites of the host lattice.[1,2] In Si,[3–5] GaAs,[6] and Ge,[7,8] the introduction of hydrogen in high concentrations results in the formation of extended planar defects, called platelets. In crystalline Si hydrogenated from a plasma at moderate temperatures, these structures are oriented predominantly along {111} crystallographic planes.[3,5] One of the most remarkable properties of the {111} platelets is their two dimensionality over diameters of many tens of nanometers while having a thickness of only a few Å.[7,9]

Polarization-sensitive Raman-scattering studies on Si samples hydrogenated from a plasma revealed the existence of at least two different modifications of {111} platelets, which coexist in concentrations depending on the hydrogenation conditions.[5] At low hydrogenation temperatures, an optically dense structure characterized by a dielectric constant $\epsilon \approx 14$ is formed, whereas for temperatures above 100 °C, a structure with $\epsilon \approx 1$ containing molecular hydrogen dominates.[5]

These experimental results are in agreement with theoretical calculations, which found that the double layer of H_2^* aggregates, $[H_2^*]_n^D$, has the lowest energy of all proposed models for the {111} platelets.[10] More recent investigations suggested that for small lattice dilations the half-stacking fault structure is even more stable.[11]

For further lattice dilations, the $[H_2^*]_n^D$ configuration transforms into the $[2Si-H+H_2]_n$ structure, where each Si–Si bond in a [111] direction is replaced by two Si–H bonds with H_2 being trapped between the two hydrogenated Si layers.[11,12] The $[2Si-H+H_2]_n$ structure is the most plausible candidate for the platelets with $\epsilon \approx 1$ containing molecular hydrogen, which will be discussed in this paper.

Molecular hydrogen consists of two protons with nuclear spin 1/2, thus obeying the Pauli principle requiring the total wave function of the system to be antisymmetric with respect to the permutations of the nuclei. The total nuclear spin I of the molecule is either 0, referred to as para H_2, or 1, referred to as ortho H_2. Since the nuclear-spin wave function of the para (ortho) configuration is antisymmetric (symmetric), the rotational wave function must be symmetric (antisymmetric), thus allowing only even (odd) values for the rotational quantum number J.[13]

The conversion from the ortho state with $J=1$ to the para ground state with $J=0$ is not possible for an isolated H_2. The presence of a nearby magnetic moment, however, renders this transition allowed[14] and it has been observed in various systems such as solid H_2,[15–19] H_2 adsorbed on surfaces,[20–23] or H_2 in the liquid and gaseous phase.[24]

Raman-scattering studies of hydrogenated Si showed that the stretch local vibrational modes (LVMs) of H_2 trapped within platelets result in a broad band around 4150 cm^{-1},[25,26] which is very close to the corresponding frequencies of free H_2.[27] Fukata *et al.*[25] and Leitch *et al.*[28,29] observed the stretch LVMs of H_2 within platelets to consist of two components around 4130 and 4160 cm^{-1} and found that the intensity ratio of these components depends on the thermal history of the sample.

Fukata *et al.* state that the width of the vibrational Raman line of H_2 does not change with the measurement temperature down to 90 K,[25] whereas Leitch *et al.* observed a decrease in line width from 26 cm^{-1} (RT) to 18 cm^{-1} (7.5 K) while the general shape remained the same.[28,29] Job *et al.* describe the H_2 vibrational Raman line as consisting of three components around 4140, 4150, and 4160 cm^{-1}.[30,31] They assigned the signals at 4150 and 4160 cm^{-1} to ortho H_2 and para H_2 trapped in platelets, respectively, whereas the broader component around 4140 cm^{-1} was attributed to hydrogen molecules located in smaller voids/platelets or precursors of platelets.[30,31]

In addition to the stretch LVMs, a weak line at around 590 cm^{-1} in the Raman spectra of hydrogenated Si was previously reported and associated with the $S_0(1)$ transition of H_2.[25] Here, $S_0(J)$ denotes the purely rotational transition $J \rightarrow J+2$ in the vibrational ground state.

In the present study, we get further insight into the properties of the two-dimensional molecular hydrogen trapped within {111} platelets in Si. We identify rotational transitions of the molecule, investigate ortho-to-para (o-p) and para-to-ortho (p-o) back conversion processes at different temperatures; and identify the contributions of ortho and para H_2 in the stretch mode of H_2 at around 4150 cm^{-1}.

II. EXPERIMENTAL PROCEDURE

The samples used in this study were n type, P-doped (100) Cz Si wafers with a resistivity of 0.75 Ω cm. They

were hydrogenated in a remote RF (13.56 MHz) plasma at a temperature of about 220 °C. The gas pressure was held at 2 mbar.

To investigate the ortho-to-para conversion at low temperatures, the sample was stored in the dark at 77 K in liquid nitrogen (LN_2) or at $T \leq 20$ K employing liquid helium (LHe). For the para-to-ortho back conversion, the sample was stored in the dark at 300 ± 1 K in air.

Raman measurements were performed in a pseudobackscattering geometry using the frequency doubled 532 nm line of a $Nd:YVO_4$ laser for excitation. For this wavelength, the estimated probing depth $\frac{1}{2\alpha}$ in our experiment is about 410 nm.[32] The incident laser beam made an angle of 40° with the sample normal. The excitation light was focused on a spot size of about 50 μm $\times$ 5 mm using a cylindrical lens.

The backscattered light was analyzed using a single grating spectrometer and a LN_2 cooled Si charge coupled device detector array. Spectral resolution varied between 2 and 4 cm^{-1}. The measurements were performed with the sample mounted in a cold finger cryostat using LHe for cooling.

During the measurements, the temperature in the bulk of the sample, T_{bulk}, was varied by an electrical heater. The actual temperature within the excitation area, T_{act}, however, was different from T_{bulk}, and was determined from the Stokes to antiStokes ratio of the Si phonon line at 521 cm^{-1}. This allowed us to control temperatures down to approximately 60 K since for lower temperatures the antiStokes intensity was too low to determine. For temperatures below 60 K, T_{act} was estimated by extrapolation of the functional dependence of T_{bulk} vs T_{act}.

The scattering geometry is defined with respect to the (100) sample surface: The x, y, and z axes are parallel to the crystallographic orientations [100], [010], and [001], respectively, whereas the x', y', and z' axes are set to be parallel to [100], [011], and $[0\bar{1}1]$, respectively.

In the notation $a(b,c)d$, $a(d)$ refers to the propagation vector of the incident (scattered) light, whereas $b(c)$ characterizes the polarization vector of the incident (scattered) light. The depolarization ratio, Δ, is defined as the ratio of the intensity of the scattered light polarized perpendicular to the incident light, to the intensity of the scattered light polarized parallel to it. In the notation $\Delta_{[xyz]}$, the subscript implies that the excitation light is polarized along the $[xyz]$ axis.

III. RESULTS

A. H_2 rotational modes

The Raman spectrum of a hydrogenated Si sample obtained at RT is shown in Fig. 1 (top). The Raman spectra in this spectral region are dominated by the Si phonon transition at 521 cm^{-1} and other intrinsic phonon modes. For better clarity, the spectrum of hydrogenated Si sample was background corrected by subtracting the reference spectrum recorded on a virgin Si sample. As follows from the figure, the hydrogenation gives rise to lines at 353(1), 587(1), 815(1), and 1034(2) cm^{-1} labeled $S_0(0)$, $S_0(1)$, $S_0(2)$, and $S_0(3)$, respectively.

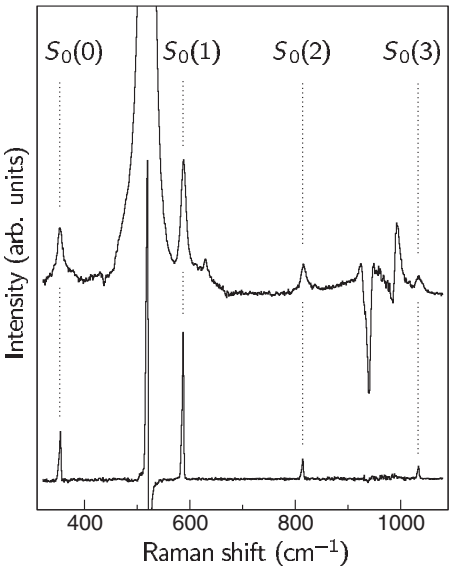

FIG. 1. Top: RT Raman spectrum of a (100)-Si sample after exposure to a hydrogen plasma. Bottom: RT spectrum of gaseous H_2. Spectral resolution was 4 cm^{-1}. Spectra are background corrected by subtracting the spectrum of a virgin Si sample.

Identification of these transitions comes from the comparison with the spectrum recorded on gaseous H_2 presented in the bottom of Fig. 1. It was obtained by filling the cryostat with H_2 gas under a pressure of 1 bar, using virgin Si as a background. Note that the features not labeled result from the nonideal subtraction of the reference spectrum.

Comparison of the two spectra in Fig. 1 shows that the lines at 353, 587, 815, and 1034 cm^{-1} should be assigned to the rotational transitions $S_0(0)$, $S_0(1)$, $S_0(2)$, and $S_0(3)$ of H_2, respectively.[27] Here, $S_0(J)$ denotes the purely rotational transition $J \rightarrow J+2$. The errors quoted result from the error in the alignment of the spectrometer obtained by comparison of the measured positions of the rotational transitions of H_2 with the tabulated ones. We note that a weak line at around 590 cm^{-1} in the Raman spectra of hydrogenated Si was previously also reported and associated with the $S_0(1)$ transition of H_2.[25]

In order to obtain more information about the rotational transitions of H_2 in Si, isotope substitution experiments using deuterium would be desirable. Due to the reciprocal dependency of the rotational energy of a diatomic molecule on the reduced mass, the most intense transitions $S_0(0)$ and $S_0(1)$ are expected to be positioned at 179 and 298 cm^{-1}, respectively.[27] The limitations of our Raman setup and overlap of the corresponding modes with the strong Si phonon background, however, did not allow us to detect the rotational transitions of D_2.

Molecular hydrogen can be located at various sites of the Si host lattice: at interstitial T sites;[26,33–35] bound at oxygen;[33,36–38] trapped within voids;[39,40] or within hydrogen-induced platelets.[5,9,26] The fact that the frequencies and intensity ratios of the rotational modes of H_2 observed in the top spectrum of Fig. 1 are very close to those of free H_2 indicates that this species should be isolated from the Si host. This rules out isolated T sites, interstitial oxygen, and voids

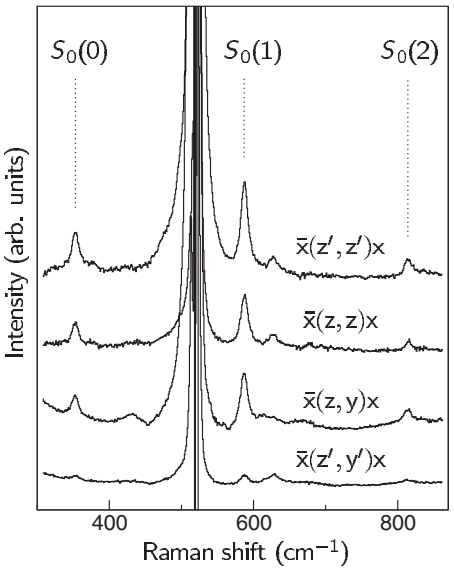

FIG. 2. RT polarization sensitive Raman spectra of (100)-Si after exposure to a hydrogen plasma. Spectra are background corrected by subtracting the spectrum of a virgin sample. Spectral resolution was 4 cm^{-1}.

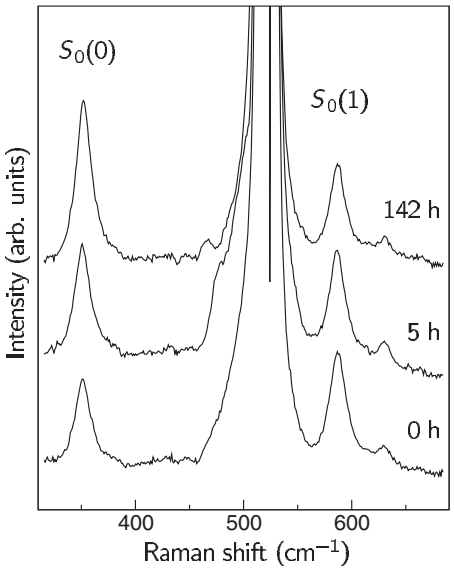

FIG. 3. Raman spectra of (100)-Si after exposure to a hydrogen plasma and subsequent storage in LN_2, measured at 95 K: Right after hydrogenation, and after storing the sample at 77 K for 5 h, and 142 h. Spectra are background corrected by subtracting the spectrum of a virgin sample. Spectral resolution was 4 cm^{-1}.

as possible traps for the molecule resulting in the $S_0(J)$ rotational modes. At these sites, H_2 is known to strongly interact with the host atoms, which gives rise to a significant redshift of the stretch modes of H_2 from the value of around 4160 cm^{-1} observed for the free species.[27]

Contrary to that, H_2 trapped within {111} platelets was shown to have a stretch mode at 4150 cm^{-1}, which is close to that of free H_2.[5,26] We found that the rotational $S_0(J)$ modes always appear together with the platelet signal at 4150 cm^{-1}. This suggests that the two sets of Raman signals have the same origin.

The polarization sensitive Raman spectra presented in Fig. 2 provide a strong support for the assignment of the 353, 587, 815, and 1034 cm^{-1} lines to the rotational modes of H_2 trapped within {111} platelets. The figure clearly shows that the intensities of these lines depend on the sample orientation with respect to the $\boldsymbol{E}_0$ vector of the excitation light and the orientation of the polarizer. In particular, the intensities of the 353, 587, and 815 cm^{-1} lines have the maximum value in the $\bar{x}(z',z')x$ geometry and nearly disappear from the spectrum being measured in the $\bar{x}(z',y')x$ geometry. In terms of depolarization ratio the results presented in Fig. 2 imply that $\Delta_{[100]} \approx 1$, whereas $\Delta_{[110]} \approx 0$. The same values of $\Delta_{[100]}$ and $\Delta_{[110]}$ are obtained for the stretch modes of H_2 at around 4150 cm^{-1}.[5]

Such polarization properties of vibrational and rotational modes of H_2 suggest a trigonal symmetry of the scattering species,[41] which agrees with the {111} orientation of the platelets and provides a strong support for the origin of the 353, 587, 815, and 1034 cm^{-1} lines as rotational transitions of H_2 trapped within {111} platelets. It might appear that the depolarization ratio of the freely rotating H_2 for the rotational modes should not depend on the sample orientation. For free gaseous H_2 not trapped within platelets, the depolarization ratio Δ for the rotational modes is expected to be approximately 3/4.[42] This seems to contradict our suggestion of freely rotating H_2 trapped within the platelets. The explanation for this peculiarity comes from the difference between the dielectric constants of the internal volume of the platelets and that of the bulk Si. This results in deviation of the $\boldsymbol{E}$ vector *within* the platelets from that of the incoming excitation light $\boldsymbol{E}_0$ and gives rise to the apparent trigonal symmetry of the Raman signals originating from the internal volume of these structures.[5]

A careful theoretical consideration of dipole radiation in multilayer stacks of dielectric media was considered by Reed *et al.*[43] A simplified explanation of the apparent trigonal symmetry of the freely rotating H_2 trapped within the {111} platelets is given in the Appendix.

B. Ortho-para conversion

Figure 3 shows Raman spectra of the hydrogenated Si sample obtained at 95 K after storage in LN_2. At this temperature due to the negligible thermal excitation of the $J=2$ and $J=3$ rotational states, the $S_0(2)$ and $S_0(3)$ lines are not visible in the spectra.

After a long enough storage at 300 K, the ratio of the integrated intensities of the $S_0(1)$ and $S_0(0)$ lines saturates and becomes equal to 1.4 ± 0.3. The storage at 77 K (LN_2) changes this ratio: the integrated intensity of the $S_0(1)$ line decreases, whereas the intensity of the $S_0(0)$ signal increases, thus suggesting a conversion of H_2 from the ortho-to-para nuclear-spin state. Figure 4 (top) shows the change in the ratio of the integrated intensities of the $S_0(1)$ and $S_0(0)$ Raman lines, abbreviated as I_1/I_0, with increasing storage time in LN_2.

Recently, both *o-p* and *p-o* transitions of isolated interstitial H_2 in Si have been investigated and suggested to be

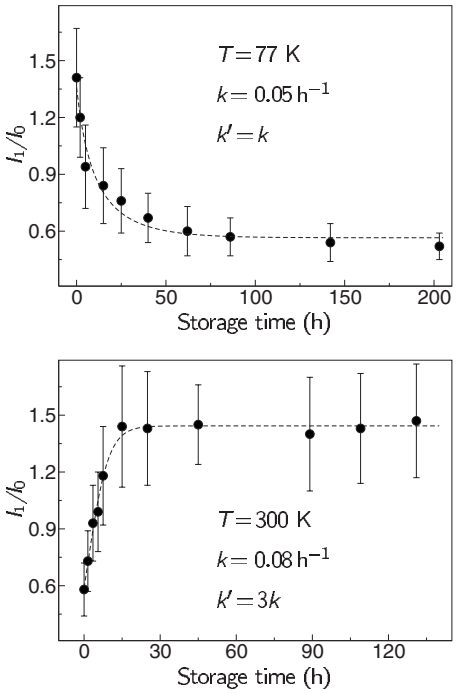

FIG. 4. Ortho-to-para ratio (I_1/I_0) as a function of storage time for storage of the sample at 77 K (top) and 300 K (bottom).

caused by interaction of H_2 with the nuclear magnetic moment of the Si isotope ^{29}Si.[44] In particular, it was found that at 77 K the equilibrium *o-p* ratio is reached after approximately 500 h. As follows from Fig. 4 (top), the I_1/I_0 ratio of H_2 trapped in platelets comes to equilibrium much faster: it saturates already after about 100 h. In our opinion, this suggests a different conversion pathway(s). In the following discussion we provide arguments in favor of interaction between neighboring H_2 as the dominant *o-p* conversion mechanism in platelets.

In thermal equilibrium, the ratio of the concentrations of ortho and para H_2 reads[45]

$$\left.\frac{n_o}{n_p}\right|_{\mathrm{eq}}(T) = 3\frac{\sum_{J=1,3,\ldots}(2J+1)\exp\{-E(J)/kT\}}{\sum_{J=0,2,\ldots}(2J+1)\exp\{-E(J)/kT\}}. \quad (1)$$

Here, $n_{o(p)}$ denotes the concentration of ortho H_2 (para H_2), the prefactor of 3 accounts for the ratio of the degeneracies of the $I=1$ and $I=0$ nuclear-spin states. The sum in the numerator is over all odd values of J, whereas the sum in the denominator runs over all even values of J.

$$E(J) = \frac{\hbar^2}{2\mu r^2}J(J+1) \quad (2)$$

denotes the rotational energy of a diatomic molecule with rotational quantum number J, where μ is the reduced mass and r is the internuclear distance.[13]

At 300 K, Eq. (1) yields $(n_o/n_p)_{\mathrm{eq}} \approx 3$, whereas in our experiment we observe $I_1/I_0 \approx 1.4 \pm 0.3$. The explanation of this "discrepancy" comes from the fact that, in addition to concentration, the intensity of a Raman line resulting from a rotational transition is given by[42]

$$I \propto \omega^4 b^{(2)}_{J+2,J} N_J, \quad (3)$$

where ω is the frequency of the scattered radiation, $b^{(2)}_{J+2,J}$ is the Placzek-Teller factor of the transition under consideration, and N_J is the number of scatterers with initial state J.

The Placzek-Teller factor for the initial ortho state with $J=1$ is $b^{(2)}_{3,1}=0.6$, whereas the factor for the initial para state with $J=0$ is $b^{(2)}_{2,0}=1$.[42] Moreover, at the measurement temperature of 95 K, 98% of all para molecules are in the $J=0$ rotational state, and thermal excitation of ortho H_2 from $J=1$ to higher rotational quantum numbers is negligible.

Taking into account the ω dependence, for the ratio I_1/I_0 of the integrated intensities of the $S_0(1)$ and $S_0(0)$ Raman lines, for a temperature of 95 K within the excitation area we finally obtain

$$\frac{I_1}{I_0}(t) \approx \left(\frac{\omega_L-\omega_1}{\omega_L-\omega_0}\right)^4 \frac{b^{(2)}_{3,1}n_o(t)}{0.98 b^{(2)}_{2,0}n_p(t)} \approx 0.58\frac{n_o}{n_p}(t), \quad (4)$$

where ω_L is the frequency of the excitation light, and ω_1 and ω_0 are the frequencies of the $S_0(1)$ and $S_0(0)$ transitions, respectively.

For $n_o/n_p=3$, Eq. (4) yields an expected value of $I_1/I_0=1.74$ for the intensity ratio of the respective rotational Raman lines, which is in reasonable agreement with the experimentally observed $I_1/I_0 \approx 1.4 \pm 0.3$. In assumption that the main *o-p* conversion mechanism is interaction between H_2 molecules, the time evolution of the ortho-H_2 concentration can be described by[24]

$$\frac{dn_o}{dt} = -kn_o^2 + k'n_o n_p = -kn_o^2 + k'n_o(1-n_o), \quad (5)$$

where k is the ortho-to-para conversion constant, whereas k' describes the reverse process. Here, we use the normalized concentrations with $n_o+n_p=1$.

In thermal equilibrium $dn_o/dt=0$, and thus we can write $k'=kn_o^{\mathrm{eq}}/(1-n_o^{\mathrm{eq}})$, where n_o^{eq} denotes the thermal equilibrium value of the ortho-H_2 concentration for a given temperature. Solution of this differential equation together with the initial condition $n_o(t=0)$ as obtained from Eq. (1) yields the time development of the *o-p* ratio $n_o/n_p(t)$, and thus the time development of I_1/I_0.

The best fit of the resulting equation to the experimental data, as represented by the dashed lines in Fig. 4, yields *o-p* conversion constants of $k=0.05 \pm 0.03$ and 0.08 ± 0.03 h^{-1} at 77 and 300 K, respectively. Note that in the fit the equilibrium values of I_1/I_0 were allowed to adjust to the experimentally observed values.

C. H_2 vibrational modes

With the results obtained in the previous sections on the rotational modes, we can now proceed with the stretch LVMs of H_2 in platelets. Figure 5 shows Raman spectra of gaseous H_2 (bottom) and H_2 trapped within the {111} platelets (top) taken at RT. Here, $Q_1(J)$ denotes the purely vibrational transition ($\nu=0 \rightarrow \nu=1$) without changing the rotational quantum number J.

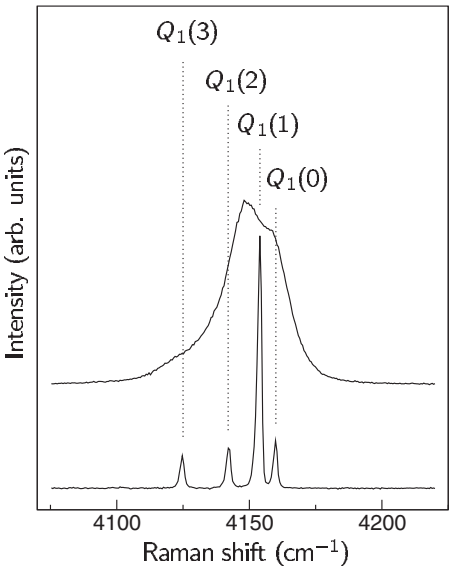

FIG. 5. Top: Raman spectrum of hydrogenated Si taken at RT. Bottom: RT Raman spectrum of gaseous H_2.

As can be seen from the figure, the broad band around 4150 cm^{-1} assigned to the vibrational modes of H_2 trapped in platelets consists of several components. Fukata *et al.*[25] and Leitch *et al.*[28,29] observed the vibrational modes of H_2 within platelets to consist of two components around 4130 and 4160 cm^{-1}, the intensity ratio of which depends on the thermal history of the sample.

As mentioned already, Job *et al.* reported that the H_2 vibrational Raman band consists of three components with frequencies of about 4140, 4150, and 4160 cm^{-1}.[30,31] These authors assigned the signals at 4150 and 4160 cm^{-1} to ortho and para H_2 trapped within platelets, respectively. The line at 4140 cm^{-1} was associated to H_2 located in very small voids/platelets or precursors of platelets.[30,31] This assignment, however, meets serious difficulties.

The frequencies of both the vibrational and rotational transitions of H_2 trapped within platelets are essentially the same as those of gaseous H_2 (see Figs. 1 and 5). This means that the hydrogen molecules within platelets are weakly coupled to the Si host lattice. On the other hand, Job *et al.*[30,31] suggest the splitting between the $Q_1(0)$ mode of para H_2 and the $Q_1(1)$ mode of ortho H_2 to be as big as 10 cm^{-1}, which significantly differs from the value of 6 cm^{-1} as detected for free H_2.[27] Moreover, these authors have found that the intensity ratio of the Raman lines at 4150 and 4160 cm^{-1} is different for equally prepared and measured *n*-type and *p*-type Si (see, e.g., Fig. 2 in Ref. 30 or Fig. 3 in Ref. 31). The *o-p* ratio, however, should only depend on the thermal history of the sample and on the measurement temperature.

In the previous section we showed that *o-p* conversion of H_2 within platelets occurs during storage of the sample at low temperatures. We want to use this property to clarify the origin of the stretch LVMs of H_2 in platelets.

Figure 6 shows low-temperature Raman spectra of the rotational transitions $S_0(0)$ and $S_0(1)$ and stretch modes of H_2 trapped in platelets after (a) storage of the sample at 300 K, (b) at 77 K for 6 days, and (c) at about 20 K for roughly one month. The temperature within the laser-excitation area was estimated to be approximately 20 K.

The ortho-to-para equilibrium ratio, $n_o:n_p$, as determined from Eq. (1) is $n_o:n_p \approx 3:1$, 2:2, and 0:4 for 300, 77, and 20 K, respectively. Figure 6 (left panel) depicts the change in the thermal equilibrium *o-p* ratio with the sample storage temperature using the rotational modes of H_2 as a probe. The storage time at each temperature was long enough to ensure that $n_o:n_p$ reaches equilibrium (see Fig. 4). From the spectrum (c) in the left panel of the figure and Eq. (4) we estimate

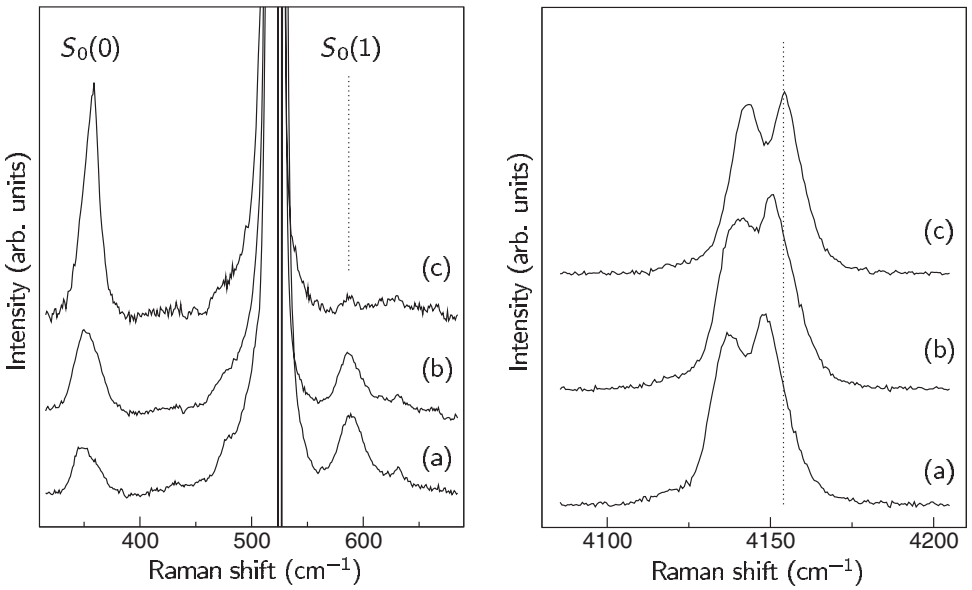

FIG. 6. Raman spectra of (100)-Si after exposure to a hydrogen plasma: (a) right after hydrogenation, (b) after subsequent storage in LN_2 for 6 days, and (c) after subsequent storage in LHe ($T \leq 20$ K) for roughly one month. Spectra are background corrected by subtracting the spectrum of a virgin sample, spectral resolution was 2 cm^{-1}. The temperature in the laser excitation area was approximately 20 K.

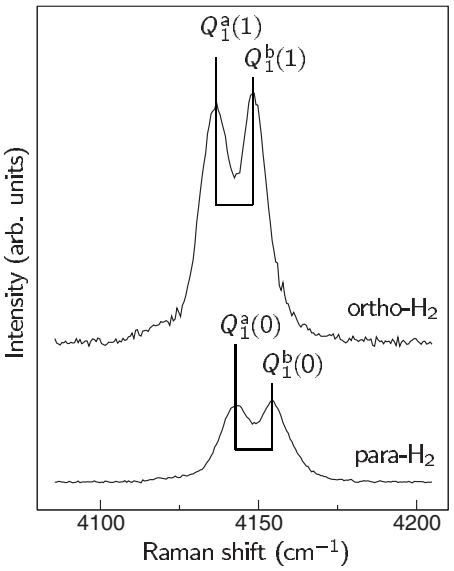

FIG. 7. Raman spectrum of para H_2 (see Fig. 6) and decomposed spectrum of ortho H_2 (see text) trapped in {111} platelets. $n_o:n_p=3:1$. The measurement temperature was approximately 20 K.

that after storage in LHe the ortho-H_2 fraction is less than 8% of the total hydrogen concentration.

Surprisingly, from spectrum (c) in the right panel of Fig. 6 one can see that even in the case of nearly pure para H_2 ($n_o:n_p \approx 0:4$) the vibrational Raman line originating from H_2 in platelets consists of at least two components at 4143 and 4154 cm^{-1}. Since at the measurement temperature of approximately 20 K excitation of para H_2 to rotational quantum numbers higher than $J=0$ can be neglected, these two lines have to be assigned to $Q_1(0)$ modes of different para-H_2 species. We suggest that these species come from different types of platelets and label these as Type *A* and Type *B*. The corresponding stretch LVMs are denoted as $Q_1^a(0)$ and $Q_1^b(0)$, respectively.

Figure 6 (right panel) depicts the change in the Raman spectra of the vibrational modes of H_2 with changing *o-p* ratio. As the fraction of ortho H_2 grows, the observed peak positions shift to the low-frequency side of the spectrum. From these spectra and the known *o-p* ratio the spectrum of pure ortho H_2 can be easily extracted. The result is shown in Fig. 7. Similar to the case of pure para H_2, we find that the low-temperature spectrum of pure ortho H_2 consists of two peaks at 4137 and 4148 cm^{-1}, which are assigned to $Q_1(1)$ modes of different ortho-H_2 species. We label these two modes $Q_1^a(1)$ and $Q_1^b(1)$, respectively.

Our assignment of the vibrational modes of H_2 in {111} platelets is supported by the splitting of $Q_1^a(0)-Q_1^a(1)=Q_1^b(0)-Q_1^b(1)=6$ cm^{-1}, which coincides with the ortho-para splitting of the $Q_1(0)$ and $Q_1(1)$ modes of unperturbed gaseous H_2.[27]

We also note that the splitting between vibrational modes due to different platelet types, $Q_1^b(0)-Q_1^a(0)=Q_1^b(1)-Q_1^a(1)\approx 11$ cm^{-1}, is very close to the splitting of 10 cm^{-1} between the lines at 4150 and 4160 cm^{-1} as reported by Job *et al.* The shoulder on the low-frequency side of the H_2 vibrational spectra measured at RT, as observed by Job *et al.* and as also visible in Fig. 5, can be explained by thermal excitation to higher rotational levels [see modes $Q_1(2)$ and $Q_1(3)$ in Fig. 5].

TABLE I. Vibrational and rotational transitions of H_2 in {111} platelets in Si (cm^{-1}). The values for free H_2 are given for comparison.

Species	$S_0(0)$	$S_0(1)$	$S_0(2)$	$S_0(3)$	$Q_1(0)$	$Q_1(1)$
Type *A*	353	587	815	1034	4143	4137
Type *B*	353	587	815	1034	4154	4148
Free H_2	354	587	814	1035	4161	4155

The frequencies of rotational and stretch LVMs of H_2 trapped in {111} platelets are summarized in Table I. The modes of free H_2 are given for comparison.

For the sake of completeness we note that the Si–H stretch modes around 2100 cm^{-1} accompanying the formation of hydrogen-induced platelets[4,5,25,28,30,31] were also investigated (spectra not shown). No influence of the *o-p* ratio on these signals was found.

IV. DISCUSSION

In the previous sections the *o-p* conversion rate of H_2 in platelets at different temperatures was investigated. This helped us to distinguish between ortho-H_2 and para-H_2 vibrational modes and to identify two types of platelets, which differ in the vibrational mode frequencies by $\Delta\omega_q=11$ cm^{-1}. On the other hand, only one rotational mode for each $S_0(J)$ transition was found.

Energetic and vibrational frequencies of interstitial H_2 molecules in different semiconductors were theoretically considered in Ref. 46. The force constant κ was found to be a linear function of the H–H bond length, *r*.

Vibrational modes of a harmonic oscillator are proportional to $\sqrt{\kappa}$, whereas frequencies of rotational transitions depend on the bond length as r^{-2}. From here, and the dependency κ vs *r* determined in Ref. 46, the splitting between rotational modes, $\Delta\omega_s$, can be estimated. For $\Delta\omega_q=11$ cm^{-1} we get that $\Delta\omega_s$ should be less than 2 cm^{-1}. Taking into account that the full width at half maximum of the Raman lines is around 10 cm^{-1}, we conclude that it is very hard to distinguish between the two types of platelets from the rotational transitions of H_2. This also implies that a separate investigation of the *o-p* conversion rate for the two types of platelets is not possible at present.

A question arises as to the origin of the two (at least) types of {111} platelets in Si. A likely explanation follows from the difference in vibrational modes of H_2: the platelets must differ in the coupling strength of the molecule with neighboring H_2 and/or Si host. The latter assumes different platelet thickness, the former—different H_2 density. For a definite solution, however, further studies and possibly support from theoretical calculations are required.

Insight into the density of H_2 can be obtained from high-resolution transmission electron microscopy (TEM) studies.[7]

A pressure of 1.4 GPa within platelets at room temperature was reported. Assuming that it is due to the gaseous hydrogen, one can estimate its density, ρ. From the equation of state of hydrogen,[47] we obtain that $\rho \approx 0.155$ g/cm^3 which corresponds to the concentration of 5×10^{22} cm^{-3}. For comparison: the density of H_2 at the triple point is 0.077 g/cm^3.[32]

Ortho-para conversion in liquid and gaseous hydrogen for densities up to 0.09 g/cm^3 and temperatures from 14 to 120 K was investigated in Ref. 24. Consequently, an interpolation formula for the *o-p* conversion rate was proposed as a function of the hydrogen density and the temperature. Applying the equation

$$k = A(T)\rho + C(T)\rho^{4.2}, \tag{6}$$

which is consistent with the parameters as determined in Ref. 24 for $\rho = 0.155$ g/cm^3, the extrapolated *o-p* conversion rate yields $k \approx 0.05$ and 0.08 h^{-1} at 77 and 300 K, respectively. These values basically coincide with those obtained in Sec. III B for H_2 trapped in platelets. Thus, the *o-p* conversion rate is consistent with the hydrogen density obtained from the TEM studies and supports our suggestion that the dominant conversion mechanism in platelets is interaction between the neighboring H_2 molecules.

In addition to temperature and density, the *o-p* conversion rate also depends on the state of matter of hydrogen.[24] The high concentration of H_2 in platelets suggests that at sufficiently low temperatures a phase transition gas-to-liquid and/or liquid-to-solid might occur. The two dimensionality of the H_2 gas in platelets as well as interaction with the Si host should determine the transition temperature(s).

At present, we are vague about the state of matter of hydrogen in platelets in the temperature range 20 to 300 K considered in this study. Further experiments are planned to address this issue.

V. SUMMARY

Properties of molecular hydrogen trapped within {111}-oriented platelets in Si were investigated by means of Raman scattering. The rotational transitions $S_0(J)$ with $J=0,1,2,3$ were identified and investigated. At low temperatures, ortho-to-para conversion of H_2 trapped within platelets has been observed and suggested to be due to interaction of nearby ortho-H_2 molecules. The ortho-to-para transition rate was found to be 0.05 ± 0.03 and 0.08 ± 0.03 h^{-1} at temperatures 77 and 300 K, respectively. The contributions of the ortho and para species to the band originating from the vibrational transitions of H_2 within platelets were separated. Two types of platelets were identified with vibrational modes at 4143 and 4154 cm^{-1} (4137 and 4148 cm^{-1}) assigned to two different species of para H_2 (ortho H_2).

ACKNOWLEDGMENTS

This work was supported by the Deutsche Forschungsgemeinschaft under Grant No. LA 1397/3.

APPENDIX: DEPOLARIZATION RATIO

Dipole radiation in multilayer stacks of dielectric media was considered by Reed *et al.*[43] The method proposed by these authors was successfully employed in Raman-scattering studies of {111} platelets in Si and Ge.[5,8]

The purpose of this appendix is to provide an explanation for the apparent trigonal symmetry of the Raman signals of the freely rotating H_2 trapped within the {111} platelets without using the elaborate mathematical formalism developed by Reed *et al.*

The key to understand the polarization properties of H_2 trapped within the platelets is a difference in dielectric constants inside the platelets, ϵ, from that of the bulk of the semiconductor, ϵ_0.

From the boundary conditions of the Maxwell equations, the tangential and normal components of the electric field within the platelets, $\boldsymbol{E}$, and that of in the bulk of semiconductor, $\boldsymbol{E}_0$, are

$$E_t = E_{0t} \tag{A1a}$$

$$\epsilon E_n = \epsilon_0 E_{0n}. \tag{A1b}$$

Since $\epsilon_0 \gg \epsilon \approx 1$ we obtain that

$$E_n \gg E_t. \tag{A2}$$

Thus, the electric field within the platelets is practically aligned parallel to the platelet's normal.

The induced dipole moment $\boldsymbol{\mu}$ of the H_2 molecules in platelets is given by the relation

$$\boldsymbol{\mu} = \mathcal{A}\boldsymbol{E}, \tag{A3}$$

where $\mathcal{A}$ is the Raman tensor of H_2. Equation (A3) may be rewritten in more conventional form as

$$\boldsymbol{\mu} = \mathcal{A}'\boldsymbol{E}_0. \tag{A4}$$

Here, $\mathcal{A}'$ is an "effective" Raman tensor of the molecule. Because $\boldsymbol{E} \| [111]$, the effective Raman tensor is *trigonal*. That is, $\mathcal{A}'$ is diagonal in the coordinate system with one of the main axes aligned parallel to [111].

The intensity of the appropriate Raman band is given by

$$I_{[xyz]} \propto \sum_{k \in \langle 111 \rangle} |\boldsymbol{e}_{[xyz]}\boldsymbol{\mu}_k|^2, \tag{A5}$$

where the summation is taken over the four possible orientation of the {111} platelets in the lattice. Here, $\boldsymbol{e}_{[xyz]}$ is the orientation of the polarizer.

Performing all needed summations in Eq. (A5) we obtain that for H_2 in {111} platelets $\Delta_{[100]}=1$ and $\Delta_{[110]}=0$, which coincides with the values expected for a trigonal center in a cubic crystal.[41]

Thus, the apparent trigonal symmetry of H_2 in platelets comes from a difference in dielectric constants of the H_2 gas and that of the bulk of Si.

*edward.lavrov@physik.tu-dresden.de

[1] *Hydrogen in Semiconductors*, Semiconductors and Semimetals, edited by J. I. Pankove and N. M. Johnson (Academic Press, New York, 1991), Vol. 34.
[2] S. J. Pearton, J. W. Corbett, and M. Stavola, *Hydrogen in Crystalline Semiconductors* (Springer-Verlag, Heidelberg, 1992).
[3] N. M. Johnson, F. A. Ponce, R. A. Street, and R. J. Nemanich, Phys. Rev. B **35**, 4166 (1987).
[4] J. N. Heyman, J. W. Ager III, E. E. Haller, N. M. Johnson, J. Walker, and C. M. Doland, Phys. Rev. B **45**, 13363 (1992).
[5] E. V. Lavrov and J. Weber, Phys. Rev. Lett. **87**, 185502 (2001).
[6] J. R. Botha, in *Proceedings of the 24th International Conference on the Physics of Semiconductors*, Jerusalem, 1998 (World Scientific, Singapore, 1998), CD-ROM 0999.pdf.
[7] S. Muto, S. Takeda, and M. Hirata, Mater. Sci. Forum **143-147**, 897 (1994).
[8] M. Hiller, E. V. Lavrov, and J. Weber, Phys. Rev. B **71**, 045208 (2005).
[9] S. Muto, S. Takeda, and M. Hirata, Philos. Mag. A **72**, 1057 (1995).
[10] S. B. Zhang and W. B. Jackson, Phys. Rev. B **43**, 12142 (1991).
[11] N. Martsinovich, M. I. Heggie, and C. P. Ewels, J. Phys.: Condens. Matter **15**, S2815 (2003).
[12] Y.-S. Kim and K. J. Chang, Phys. Rev. Lett. **86**, 1773 (2001).
[13] G. Herzberg, *Molecular Spectra and Molecular Structure: I. Spectra of Diatomic Molecules* (Van Nostrand Reinhold, New York, 1950).
[14] E. Wigner, Z. Phys. Chem. Abt. B **23**, 28 (1933).
[15] I. F. Silvera, Rev. Mod. Phys. **52**, 393 (1980) and references therein.
[16] A. Driessen, E. van der Poll, and I. F. Silvera, Phys. Rev. B **30**, 2517 (1984).
[17] E. Ilisca and S. Sugano, Phys. Rev. Lett. **57**, 2590 (1986).
[18] M. G. Pravica and I. F. Silvera, Phys. Rev. Lett. **81**, 4180 (1998).
[19] M. A. Strzhemechny and R. J. Hemley, Phys. Rev. Lett. **85**, 5595 (2000).
[20] Y. L. Sandler and M. Gazith, J. Phys. Chem. **63**, 1095 (1959).
[21] E. Ilisca, Phys. Rev. Lett. **66**, 667 (1991).
[22] E. Ilisca and S. Paris, Phys. Rev. Lett. **82**, 1788 (1999).
[23] K. Fukutani, K. Yoshida, M. Wilde, W. A. Diño, M. Matsumoto, and T. Okano, Phys. Rev. Lett. **90**, 096103 (2003).
[24] Yu. Ya. Milenko, R. M. Sibileva, and M. A. Strzhemechny, J. Low Temp. Phys. **107**, 77 (1997).
[25] N. Fukata, S. Sasaki, K. Murakami, K. Ishioka, K. G. Nakamura, M. Kitajima, S. Fujimura, J. Kikuchi, and H. Haneda, Phys. Rev. B **56**, 6642 (1997).
[26] A. W. R. Leitch, V. Alex, and J. Weber, Phys. Rev. Lett. **81**, 421 (1998).
[27] B. P. Stoicheff, Can. J. Phys. **35**, 730 (1957).
[28] A. W. R. Leitch, V. Alex, and J. Weber, Solid State Commun. **105**, 215 (1998).
[29] A. W. R. Leitch, V. Alex, and J. Weber, Mater. Sci. Eng., B **58**, 6 (1999).
[30] R. Job, A. G. Ulyashin, and W. R. Fahrner, Solid State Phenom. **82-84**, 139 (2002).
[31] R. Job, A. G. Ulyashin, W. R. Fahrner, M.-F. Beaufort, and J.-F. Barbot, Eur. Phys. J. Appl. Phys. **23**, 25 (2003).
[32] *CRC Handbook of Chemistry and Physics*, edited by D. R. Lide (CRC Press, New York, 2001).
[33] R. E. Pritchard, M. J. Ashwin, J. H. Tucker, R. C. Newman, E. C. Lightowlers, M. J. Binns, S. A. McQuaid, and R. Falster, Phys. Rev. B **56**, 13118 (1997).
[34] R. E. Pritchard, M. J. Ashwin, J. H. Tucker, and R. C. Newman, Phys. Rev. B **57**, R15048 (1998).
[35] E. V. Lavrov and J. Weber, Phys. Rev. Lett. **89**, 215501 (2002).
[36] V. P. Markevich and M. Suezawa, J. Appl. Phys. **83**, 2988 (1998).
[37] E. E. Chen, M. Stavola, and W. B. Fowler, Phys. Rev. B **65**, 245208 (2002).
[38] M. Hiller, E. V. Lavrov, and J. Weber, Phys. Rev. B **74**, 235214 (2006).
[39] K. Ishioka, M. Kitajima, S. Tateishi, K. Nakanoya, N. Fukata, T. Mori, K. Murakami, and S. Hishita, Phys. Rev. B **60**, 10852 (1999).
[40] T. Mori, K. Otsuka, N. Umehara, K. Ishioka, M. Kitajima, S. Hishita, and K. Murakami, Physica B **302-303**, 239 (2001).
[41] M. Cardona, in *Light Scattering in Solids*, edited by M. Cardona and G. Güntherodt (Springer-Verlag, Berlin, 1982), Vol. II.
[42] D. A. Long, *The Raman Effect: A Unified Treatment of the Theory of Raman Scattering by Molecules* (John Wiley and Sons, New York, 2002).
[43] C. E. Reed, J. Giergiel, J. C. Hemminger, and S. Ushioda, Phys. Rev. B **36**, 4990 (1987).
[44] M. Hiller, E. V. Lavrov, and J. Weber, Phys. Rev. Lett. **98**, 055504 (2007).
[45] L. D. Landau and E. M. Lifshitz, *Statistical Physics, Part 1* (Pergamon Press, London, 1958).
[46] C. G. Van de Walle, Phys. Rev. Lett. **80**, 2177 (1998).
[47] M. Tkacz and A. Litwiniuk, J. Alloys Compd. **330-332**, 89 (2002).